

Total-Variation - Fast Gradient Flow and Relations to Koopman Theory

Ido Cohen · Tom Berkov · Guy Gilboa

November 30, 2021

Abstract The space-discrete *Total Variation* (TV) flow is analyzed using several mode decomposition techniques. In the one dimensional case, we provide analytic formulations to *Dynamic Mode Decomposition* (DMD) and to *Koopman Mode Decomposition* (KMD) of the TV flow and compare the obtained modes to TV spectral decomposition. We propose a computationally efficient algorithm to evolve the one-dimensional TV flow. A significant speedup by three orders of magnitude is obtained, compared to iterative minimizations. A common theme, for both mode analysis and fast algorithm, is the significance of phase transitions during the flow, in which the subgradient changes.

We explain why applying DMD directly on TV-flow measurements cannot model the flow or extract modes well. We formulate a more general method for mode decomposition that coincides with the modes of KMD. This method is based on the linear decay profile, typical to TV-flow. These concepts are demonstrated through experiments, where additional extensions to the two-dimensional case are given.

Keywords Isotropic and Anisotropic *Total Variation* · *Total Variation*-flow · *Total Variation*-spectral decomposition · *Dynamic Mode Decomposition* · Time Reparametrization · *Koopman Mode Decomposition*

We acknowledge support by grant agreement No. 777826 (NoMADS), by the Israel Science Foundation (Grant No. 534/19) and by the Ollendorff Minerva Center.

I. Cohen
Tel.: +927-4-829-5743
E-mail: idoc@campus.technion.ac.il

T. Berkov
E-mail: ptom@campus.technion.ac.il

G. Gilboa
E-mail: guy.gilboa@ee.technion.ac.il

List of abbreviations

ADMM	<i>Alternating Direction Method of Multipliers</i>
DMD	<i>Dynamic Mode Decomposition</i>
FGD	<i>Fastest Gradient Descent</i>
KEF	<i>Koopman Eigenfunction</i>
KMD	<i>Koopman Mode Decomposition</i>
PDE	<i>Partial Differential Equation</i>
RDMD	<i>Rescaled Dynamic Mode Decomposition</i>
SVD	<i>Singular Vector Decomposition</i>
TV	<i>Total Variation</i>

List of variables

$P(\cdot)$	a proper nonlinear operator
$\psi(t)$	The solution of a nonlinear PDE
t	The time variable
$t(\psi)$	The inverse function from the observations ψ back to the time t
$\varphi_{\mathcal{K}}(\psi)$	<i>Koopman Eigenfunction</i> (KEF)
\mathbf{v}_i	A Koopman mode
$a_{\lambda_i}(t)$	The decay profile typical to the dynamical system
J_{TV}	Total variation
J_{iso}	Isotropic total variation
J_{ani}	Anisotropic total variation
T_i	The time point at which the subgradient of TV-flow changes for the i th time.
p	a negative subgradient
p_i	The negative subgradient of the TV-flow for $t \in [T_i, T_{i+1})$
p^i	The negative subgradient in the i th extremum of the signal
$p^{(i)}$	The value of the i th pixel in the negative subgradient
p	
τ	The reparametrized time variable
φ_i	TV spectral component
ξ_1, ξ_2	Modes resulting from the rescaled TV-flow
ϕ_1, ϕ_2	Modes resulting from DMD applied on the rescaled TV-flow

1 Introduction

Dimensionality reduction is one of the most challenging tasks in data analysis. For flows, the general aim is to find a low dimensional representation of the spatial data (modes) and the corresponding temporal evolution [35]. This

allows much better understanding and facilitates fast and efficient processing of the signal. The spatio-temporal decomposition is commonly used in many disciplines such as fluid dynamics, signal analysis and computational physics, to name a few. In this work, we bridge between the TV spectral decomposition from signal processing and its connection to Koopman theory and its applications.

In order to study nonlinear dynamics, Koopman theory [26] is increasingly employed. It allows a linear representation of nonlinear flows, also referred to as KMD [29]. Since in the general case the representation is infinite-dimensional, in practice, a finite dimensional approximation is used. In fluid dynamics, *Dynamic Mode Decomposition* (DMD) is a data-driven method to approximate KMD [31]. Since DMD approximates a linear dynamical system it can be viewed as an exponential data fitting algorithm [2]. DMD has become a popular and practical analysis tool, however, it suffers from some inherent flaws [17, 18, 30, 20]. These drawbacks are emphasized in zero-homogeneous evolutions such as the TV flow.

The TV functional has been extensively used in image processing and computer vision, as it allows the preservation of edges (discontinuities). The respective steepest descent, termed TV-flow, has been studied thoroughly in the last two decades [1, 33, 32, 7, 11, 4, 1, 3]. A list of the main attributes of TV flow in a one-dimensional signal is summed up in [6]. Two of its main attributes are that the flow decays piecewise linearly and that it has a finite support in time. The above studies lay the foundation to the TV nonlinear spectral framework (spectral TV) [22, 23, 10, 24, 9, 5, 21]. A main challenge in accurately using TV flow is the computational load in calculating the subgradient. For an accurate calculation, often a convex optimization problem (such as [11]) is solved at each step. In order to obtain a full spectral TV decomposition of a signal, one has to compute the entire TV flow until extinction. This motivates us to explore fast methods to accomplish the task.

In this work, we apply the theory of Koopman operator and its applications on the TV-flow. We begin by formulating the analytic solution of TV-flow for one-dimensional signals and propose a fast algorithm to solve the flow. We first examine *Rescaled Dynamic Mode Decomposition* (RDMD) [15] which was recently proposed as an improved version of DMD for homogeneous flows (such as p -Laplacian flows [27], where the operator of the dynamics is homogeneous of degree $p - 1$). However, since there are subgradient phase transitions in TV-flow, RDMD is limited. To address this problem we suggest a new piecewise mode decomposition technique. It is based on the linear decay profile typical to the flow. We show it coincides with KMD and can perfectly model the dynamics through piecewise linear segments. We show the direct relations of the obtained modes to spectral TV decomposition [23]. A shorter version of this work was first presented in a conference [16]. Here, additional theory and experiments are shown, and a two-dimensional extension is presented.

2 Preliminaries

In this section, we summarize the definitions and methods relevant to this work.

2.1 Koopman Eigenfunctions

Let us consider the following nonlinear dynamical system

$$\frac{d}{dt}\psi = P(\psi), \quad (1)$$

where $P(\cdot)$ is a proper nonlinear operator. The observation ψ belongs to \mathbb{R}^M . We also denote the time derivative with the subscript $\{\cdot\}_t$ for simplicity.

Let $g : \mathbb{R}^M \rightarrow \mathbb{R}$ be a measurement of ψ . Bernard Osgood Koopman argued that a Hamiltonian system has measurements evolving linearly under the dynamical regime [26]. These measurements, termed as *Koopman Eigenfunctions* (KEFs), admit the following relation,

$$\frac{d}{dt}\varphi_{\mathcal{K}}(\psi(t)) = \lambda\varphi_{\mathcal{K}}(\psi(t)), \quad (2)$$

where $\varphi(\psi)$ is a KEF and λ is the respective eigenvalue. Recently, part of the authors formulated necessary and sufficient conditions for the existence of such measurements [18]. It was shown that if the solution of the system, $\psi(t)$, is injective then the measurement φ gets the form of,

$$\varphi_{\mathcal{K}}(\psi) = \varphi_{\mathcal{K}}(\psi(0))e^{\lambda t(\psi)}, \quad (3)$$

where $t(\psi)$ is the inverse function from the observations ψ back to the time t . For further details see [18].

2.2 Koopman Mode Decomposition

Koopman Mode Decomposition (KMD) is a representation of dynamical systems based on KEFs [29]. Namely, the state space ψ can be expressed as,

$$\psi(t) = \sum_{i=1}^{\infty} \mathbf{v}_i \varphi_{\mathcal{K}_i}(t), \quad (4)$$

where $\varphi_i(t)$ is a KEF and \mathbf{v}_i is the corresponding vector, referred to as Koopman mode. When the dynamic is nonlinear the decomposition may be infinite. In practice, a finite approximation method is used. The most common one is DMD.

2.3 Dynamic Mode Decomposition

Dynamic Mode Decomposition (DMD) is a data-driven algorithm to approximate KMD. Given a set of samples of the dynamic, a linear relation is formulated that approximates the generating process of the set. Commonly, the formulation is performed in a lower dimensional space. The output is triplets representing the main spatial structures (modes), their amplitudes (coefficients), and the respective time changes (eigenvalues). To recap, the three main steps of this algorithm are: 1. *Dimensionality reduction*, 2. *Optimal linear mapping*, and 3. *System reconstruction*. The output is *modes, eigenvalues and coefficients* [31].

2.4 Decay profile profile decomposition with Koopman modes

We summarize below a different decomposition method, suggested in [18], which is relevant to this work. Let us assume that the dynamical system can be formulated as,

$$\psi(t) = \sum_{i=1}^L \mathbf{v}_i a_{\lambda_i}(t), \quad (5)$$

where $a_{\lambda_i}(t)$ is the decay profile typical to the dynamical system and characterized by a parameter (or set of parameters) λ_i and \mathbf{v}_i is a spatial structure. In matrix notations,

$$\psi(t) = V \mathbf{a}_{\lambda}(t), \quad (6)$$

where $\mathbf{a}_{\lambda}(t) = [a_{\lambda_1}(t) \cdots a_{\lambda_L}(t)]^T$ and V is a matrix with the modes as its columns. If the decay profile is monotone, the inverse mapping exists and can be expressed as,

$$\mathbf{t}(\psi) = \mathbf{a}_{\lambda}^{-1}((V^T V)^{-1} V^T \psi), \quad (7)$$

where $\mathbf{a}_{\lambda}^{-1}(\cdot) = [a_{\lambda_1}^{-1}(\cdot) \cdots a_{\lambda_L}^{-1}(\cdot)]^T$. Note that \mathbf{t} is a vector of inverse mapping. Therefore, the Koopman eigenfunctions are,

$$\varphi_{\kappa}(\psi) = \exp\{\mathbf{a}_{\lambda}^{-1}((V^T V)^{-1} V^T \psi)\}, \quad (8)$$

where $\mathbf{a}_{\lambda}^{-1}(\cdot) = [a_{\lambda_1}^{-1}(\cdot) \cdots a_{\lambda_L}^{-1}(\cdot)]^T$.

The general mode decomposition algorithm is data-driven. We mention here only the part in the algorithm revealing the spatial structures. For the rest of the algorithm, we refer the reader to [18]. Given the data matrix, Ψ , we initialize the decay profile dictionary, \mathcal{D} . The columns of the matrix are samples of the decay vector $\mathbf{a}_{\lambda}(t)$. We minimize the expression,

$$\|\Psi - VD\|_F^2 \quad (9)$$

over V , where V is sparse columns-wise (the subscript F denotes the Frobenius norm). Then, we construct the matrices \hat{V} and \hat{D} . \hat{V} contains the non-zero (or non-negligible) modes (vectors in V) and \hat{D} contains the respective decay profiles. Note that, the mode set $\{\mathbf{v}_i\}$ is proved to be the set of Koopman modes [18].

2.5 Total Variation Spectral Decomposition

2.5.1 TV functional

One dimensional signal. The TV functional of a one dimensional function is defined by,

$$J_{TV}(\psi) = \langle |\nabla\psi|, 1 \rangle, \quad \psi \in \mathbb{R}^M, \quad (10)$$

where ∇ is the discrete gradient operator. (for more details we refer the reader to [12]).

Two dimensional signal. For a two dimensional function, the definitions of isotropic and anisotropic TV, respectively, are,

$$\begin{aligned} J_{iso}(\psi) &= \langle \|\nabla\psi\|_2, 1 \rangle = \langle \sqrt{|D_x\psi|^2 + |D_y\psi|^2}, 1 \rangle, \quad \psi \in \mathbb{R}^{M \times K} \\ J_{ani}(\psi) &= \langle \|\nabla\psi\|_1, 1 \rangle = \langle |D_x\psi| + |D_y\psi|, 1 \rangle, \quad \psi \in \mathbb{R}^{M \times K}, \end{aligned} \quad (11)$$

where $\nabla = [D_x, D_y]^T$ is the discrete gradient operator and D_x, D_y denote the differential operators according to the Cartesian coordinate system (see e.g. [28] for a new model combining these two functionals).

2.5.2 TV-flow

The TV-flow is the gradient descent flow of the TV functional,

$$\psi_t = p, \quad \psi(t=0) = f, \quad (\mathbf{TV-flow})$$

where $-p$ belongs to the subdifferential, $-p \in \partial J_{TV}(\psi)$, defined by,

$$\partial J_{TV}(\psi) = \{p | J(\theta) - J(\psi) \geq \langle -p, \theta - \psi \rangle, \forall \theta \in \mathcal{H}\}, \quad (12)$$

and \mathcal{H} is either \mathbb{R}^M or $\mathbb{R}^{M \times K}$, depending on the dimensionality of θ . A non-linear eigenfunction, v , of p admits,

$$p(v) = \lambda \cdot v, \quad (\mathbf{EF})$$

for some non-positive $\lambda \in \mathbb{R}^-$. The solution of Eq. (**TV-flow**) initialized with an eigenfunction v is,

$$\psi(t) = (1 + \lambda t)^+ \cdot v, \quad (13)$$

where λ is the corresponding eigenvalue and $(a)^+ := \max\{a, 0\}$, $\forall a \in \mathbb{R}$.

2.5.3 TV spectral framework

The spectral decomposition of a signal, $f \in \mathcal{H}$, related to the eigenfunctions of P is based on the solution of Eq. **(TV-flow)**. The definition of the TV transform is given by [23],

$$\mathcal{G}(t) = t \frac{d^2}{dt^2} \psi(t), \quad (14)$$

where $\psi(t)$ is the solution of **(TV-flow)**. The function $\mathcal{G}(t)$ is the spectral component of the signal f at time t . For example, the transform of an eigenfunction is,

$$\mathcal{G}(t) = f \cdot t \lambda^2 \cdot \delta(1 + \lambda \cdot t), \quad (15)$$

where $\delta(\cdot)$ is the Dirac measure. We list below some *Attributes* of the semi discrete one-dimensional TV-flow and the TV spectral components:

1. The subgradient is piecewise constant with respect to t (see e.g. [10]).
2. The initial condition can be reconstructed by knowing the subgradient as a function of t (by integration).
3. The flow splits into merging events [6].
4. The average of a subgradient over the spatial variable is zero.
5. The spectrum is a finite set of delta functions, where each delta function represents a spectral component [10].
6. For a given f , the spectral component set is orthogonal [10].
7. Two adjacent points which become equal in value during the flow, will not separate [33, 3].

Settings: In this work we first note that DMD is fully discrete (time and space) whereas TV-flow and spectral TV are semi-discrete (time-continuous, spatially discrete). Thus, in order to apply DMD on a gradient descent flow we first need to sample (uniformly) with respect to the time variable t . In all cases we use Euclidean inner product and norm.

3 One dimensional TV flow, DMD, Koopman eigenfunctions and modes

3.1 Optimal calculation of one dimensional TV-flow

Let us formulate *Attribute 1* and *Attribute 2* more formally. The solution of **(TV-flow)** converges to a steady state in finite time. In this finite time, the solution is divided into L disjoint segments, $\{[T_i, T_{i+1})\}_{i=0}^{L-1}$. In each segment, the subgradient is constant,

$$-p_i \in \partial J(\psi(t)), t \in [T_i, T_{i+1}), \quad (16)$$

where for $t > T_L$ it is zero, $p_{L+1} = 0$. The solution can be expressed by (e.g. [10]),

$$\psi(t) = \psi(T_i) + (t - T_i)p_i, \quad t \in [T_i, T_{i+1}). \quad (17)$$

We propose here a fast algorithm to find a subgradient of the TV functional of a one-dimensional signal. The results of this algorithm coincide with the subgradient calculated in [33].

3.1.1 Calculating a subgradient

While there has been ongoing research on fast methods for TV regularization (e.g. [13, 19, 25]), few advances were made in fast algorithms of the TV-flow, which is required for computing spectral TV. Our proposed solution, $\psi(t) \in \mathbb{R}^M \times [0, T_L]$, is in a semi-discrete setting. The algorithm is based on the TV-flow attributes listed at the end of Section 2.5. The *Fastest Gradient Descent* (FGD) flow directly stems from the works [6, 7, 33]. We assume here Neumann boundary condition (generalization to other boundary conditions is possible).

We consider an expression for the value of TV of a piecewise monotone signal f . Let the set $\{f_i\}_{i=1}^N$ be the local extremum points of the signal and let $\{m_i\}_{i=1}^N$ be the number of pixels at every local extremum. Then, the TV value of f is,

$$J_{TV} = \sum_{i=1}^N a_i f_i, \quad (18)$$

where a_1 and a_N are,

$$a_1 = \begin{cases} 1 & f_1 \text{ is a maximum} \\ -1 & f_1 \text{ is a minimum} \end{cases} \quad a_N = \begin{cases} 1 & f_N \text{ is a maximum} \\ -1 & f_N \text{ is a minimum} \end{cases}, \quad (19)$$

and for the rest of the indices,

$$a_i = \begin{cases} 2 & f_i \text{ is a maximum} \\ -2 & f_i \text{ is a minimum,} \end{cases} \quad (20)$$

where by maximum or minimum we refer to the local notions. The value of TV can be calculated also as the inner product between the subgradient $-p$ and the signal f . In addition, we know that the subgradient is zero when the signal is monotone and two adjacent and equal pixels do not separate (Attribute 7). Then, J_{TV} of f can be calculated by,

$$J_{TV} = -\langle p, f \rangle = -\sum_{i=1}^N p^i m_i f_i, \quad (21)$$

where p^i is the negative subgradient of the i th extremum point. By variation of parameters we get,

$$-p^i = \frac{a_i}{m_i}. \quad (22)$$

Algorithm 1 Fast subgradient calculation

-
- 1: **Inputs:**
 f
 - 2: Find the extrema points of f and their respective number of pixels, $\{m_i\}$.
 - 3: Find the coefficients $\{a_i\}$ in Eqs. (19) and (20).
 - 4: Calculate the negative subgradient, p , according to Eq. (22).
 - 5: **Outputs:**
The negative subgradient p
-

In Algo. 1 we summarize the steps to find the subgradient. In Fig. 1 we illustrate Algo. 1. We calculate the subgradients (right column) of two piecewise monotone signals (left column). The upper signal has one pixel at any extremum and the lower signal has m_i pixels at the i th extremum.

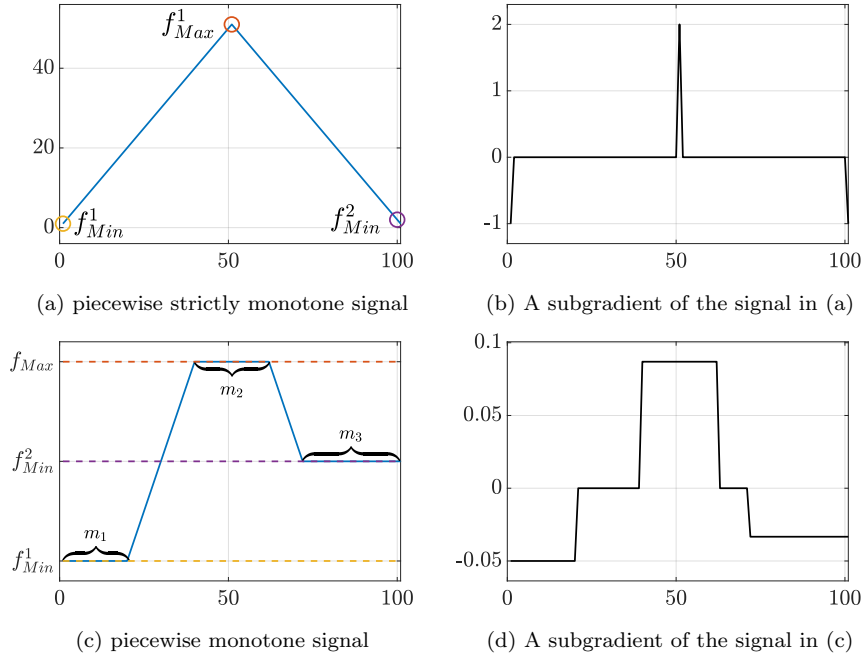


Fig. 1: **Piecewise monotonic signals** - (a) a piecewise monotone signal with one pixel at each extremum (b) its subgradient (c) a piecewise monotone signal (d) its subgradient.

Note that the subgradient depends on the relation between the pixels. Namely, the subgradient is valid as long as the number of pixels, $\{m_i\}_{i=1}^N$, and their respective extrema attribute (minimum or maximum) do not change.

3.1.2 Subgradient Updating

Let $\mathcal{T} = \{T_i\}_{i=0}^L$ be the time points at which the subgradient changes, where $T_0 = 0$, and T_L is the extinction time. These time points are when the relation among the extrema points changes. Equivalently, when the number of pixels in the extrema changes. An intersection between two adjacent pixels or number of pixels are termed *merging event*. From *Attributes 3* and *7* we can find these time points and compute the updated subgradient.

Merging event prediction: The discrete gradient approximation is $\nabla\psi^{(j)} := \psi^{(j+1)} - \psi^{(j)} = 0$, where $\psi^{(j)}$ is the entry j of the vector ψ . Using Eq. (17), the very next merging event after T_i can be calculated by

$$T_{i+1} = T_i + \min_{j \in \mathcal{J}^*} \{-\nabla\psi^{(j)}(T_i) / \nabla p^{(j)}(\psi(T_i))\}, \quad (23)$$

where

$$\mathcal{J}^* = \{j \text{ s.t. } 0 < -\nabla\psi^{(j)}(T_i) / \nabla p^{(j)}(\psi(T_i)) < \infty\}.$$

Subgradient updating: According to *Attribute 7*, the merged entries evolve together at the same pace. In addition, the subgradient at other locations is unchanged. Since the average of the subgradient is zero (*Attribute 4*), the subgradient of the merged entries is the average of the previous subgradient at these entries. Merging event prediction and subgradient updating are detailed below and concisely formalized in Algorithm 2.

Algorithm 2 Accelerated TV flow

- 1: **Inputs:**
 f
 - 2: **Initialize:** $\psi_0 \leftarrow f$, $t \leftarrow 0$, $\mathcal{T} = \emptyset$, and $\mathcal{P} = \emptyset$
 - 3: Calculate the negative subgradient, p_0 , of f by invoking Algo. 1, add p_0 to the set \mathcal{P} .
 - 4: **while** $\|p_i\| > 0$ **do**
 - 5: Find the next time transition point, T_{i+1} (Eq. (23)).
 - 6: $\psi_{i+1} \leftarrow \psi_i + (T_{i+1} - T_i) \cdot p_i$.
 - 7: Find clusters, $\{\mathcal{M}_k\}_{k=1}^r$, where $|\nabla\psi_{i+1}| = 0$
 - 8: Update the next negative subgradient, p_{i+1} , such that $p_{i+1}(\mathcal{M}_k) = \frac{1}{|\mathcal{M}_k|} \sum_{\mathcal{M}_k} p_i(\mathcal{M}_k)$, $k = 1, \dots, r$.
 - 9: Add p_{i+1} to the set \mathcal{P} ; Add T_{i+1} to the set \mathcal{T} .
 - 10: **end while**
 - 11: **Outputs:** \mathcal{T}, \mathcal{P} . The set \mathcal{P} contains the negative subgradient sequence and the set \mathcal{T} contains the transition times. Use Eq. (17) to get $\psi(t)$ for $t \in [0, T_L]$.
-

Remark 1 (TV flow - physical alegory) For one dimensional signals, the TV flow initiates every pixel with an initial velocity. Then, the rest of the flow is a series of pure plastic collisions of the pixels. Thus, the velocity of the center of mass is preserved and equals zero.

3.1.3 Closed form solution

Let us assume an initial condition, $\psi(0) = f$, is orthogonal to the kernel of J_{TV} (constant functions). The reconstruction of f from the set of negative subgradients $\{p_i\}$ is [10]

$$, f = \psi(0) = \sum_{i=1}^L T_i(p_{i+1} - p_i). \quad (24)$$

Proposition 1 (Linear decay) *The solution of (TV-flow) is a sum of spectral components decaying linearly. More formally, if the initial condition, f , is orthogonal to the kernel set of P then the solution of Eq. (TV-flow) is*

$$\psi(t) = \sum_{i=1}^L (1 + \lambda_i t)^+ \varphi_i, \text{ where } \lambda_i = -T_i^{-1} \text{ and } \varphi_i = \frac{p_i - p_{i+1}}{\lambda_i}. \quad (25)$$

Proof Let us reformulate the solution, Eq. (17) for the first time range $t \in [0, T_1]$. Substituting Eq. (24) into Eq. (17), we have

$$\begin{aligned} \psi(t) &= \psi(0) + (t - 0)p_1 = \sum_{i=1}^L T_i(p_{i+1} - p_i) + tp_1 \\ &\stackrel{p_{L+1}=0}{=} \underbrace{\sum_{i=1}^L T_i(p_{i+1} - p_i)}_{p_{L+1}=0} + t \sum_{i=1}^L (p_i - p_{i+1}) = \sum_{i=1}^L (T_i - t)(p_{i+1} - p_i). \end{aligned}$$

Therefore,

$$\psi(T_1) = \sum_{i=1}^L (T_i - T_1)(p_{i+1} - p_i) = \sum_{i=2}^L (T_i - T_1)(p_{i+1} - p_i). \quad (26)$$

In a similar manner, we can reformulate the solution for $t \in [T_1, T_2)$ as,

$$\psi(t) = \sum_{i=2}^L (T_i - t)(p_{i+1} - p_i). \quad (27)$$

By induction, the general solution is,

$$\psi(t) = \sum_{i=1}^L (T_i - t)^+(p_{i+1} - p_i). \quad (28)$$

Denoting $\lambda_i = -T_i^{-1}$, this can be expressed as,

$$\psi(t) = \sum_{i=1}^L (-\lambda_i^{-1} - t)^+(p_{i+1} - p_i) = \sum_{i=1}^L (1 + \lambda_i t)^+ \frac{p_i - p_{i+1}}{\lambda_i}. \quad \square$$

The spectral decomposition is computed by second order time derivative of $\psi(t)$ [23],

$$\mathcal{G}(t) = \sum_{i=1}^L \varphi_i \cdot t \lambda_i^2 \cdot \delta(1 + \lambda_i \cdot t). \quad (29)$$

This coincides with *Attribute 5*. A fast algorithm to find the TV spectral decomposition is proceeding Algo. 2. After finding the sets \mathcal{P} and \mathcal{T} we can calculate the spectral components $\{\varphi_i\}$ by Eq. (25).

The flow can also be defined (without using the operator $(\cdot)^+$) in disjoint time intervals,

$$\psi(t) = \sum_{i=k}^L (1 + \lambda_i t) \varphi_i, \quad \forall t \in [T_{k-1}, T_k). \quad (30)$$

We will use this formulation later in our analysis.

3.2 Rescaled-DMD

We follow the work of [15] where an analysis of DMD was carried out for flows based on homogeneous operators. The homogeneity order dictates not only the decay profile but also the support in time of the solution. In particular, TV-flow decays linearly and has a finite extinction time. However, a flow linearization algorithm, such as DMD, can be interpreted as an exponential data fitting algorithm [2] resulting in functions with infinite support. This contradiction yields an inherent error in the dynamic reconstruction by DMD. In [15] it was suggested to solve this problem by time reparameterization. Introducing a new time variable τ , Eq. (**TV-flow**) is time rescaled by the flow,

$$\psi_\tau = G(\psi) = -\frac{\langle p, \psi \rangle}{\|p\|^2} p, \quad -p \in \partial J_{TV}(\psi). \quad (\mathbf{R-TV-flow})$$

Note that, $G(a\psi) = aG(\psi)$, $\forall a \in \mathbb{R}$, i.e. G is a one-homogeneous operator. In addition, a TV eigenfunction is an eigenfunction of G , however, this eigenfunction decays exponentially under the dynamics (**R-TV-flow**). Therefore, this flow rescales only the time axis whereas the spatial axis remains unchanged. Using (**TV-flow**) and (**R-TV-flow**), the relation between t and τ can be derived by,

$$\begin{aligned} \frac{d}{d\tau} \psi(t(\tau)) &= -\frac{\langle p, \psi(t(\tau)) \rangle}{\|p\|^2} p \\ &= -\frac{\langle p, \psi(t(\tau)) \rangle}{\|p\|^2} \frac{d}{dt} \psi(t(\tau)), \end{aligned}$$

yielding,

$$\frac{d}{d\tau} t(\tau) = -\frac{\langle p, \psi(t(\tau)) \rangle}{\|p\|^2}. \quad (31)$$

This ODE gets a different form in each segment, $[T_{k-1}, T_k)$. Substituting Eq. (30) in Eq. (31), we have

$$\frac{d}{d\tau} t(\tau) = -\frac{\langle \sum_{i=k}^L \lambda_i \varphi_i, \sum_{i=k}^L (1 + \lambda_i t(\tau)) \varphi_i \rangle}{\left\| \sum_{i=k}^L \lambda_i \varphi_i \right\|^2} = -\frac{\sum_{i=k}^L \lambda_i \|\varphi_i\|^2}{\sum_{i=k}^L \lambda_i^2 \|\varphi_i\|^2} - t(\tau).$$

The solution is,

$$t(\tau) = a_k e^{-\tau} - c_k, \quad c_k = \frac{\sum_{i=k}^L \lambda_i \|\varphi_i\|^2}{\sum_{i=k}^L \lambda_i^2 \|\varphi_i\|^2}, \quad (32)$$

where a_k depends on the initial conditions of every segment such that $t(\tau)$ is continuous (where $t(0) = 0$). Then, the time points $\{T_i\}_{i=1}^L$ are mapped to $\{\tau_i\}_{i=1}^L$, accordingly.

Proposition 2 (Main TV-flow modes) *In every disjoint k th interval, $[\tau_{k-1}, \tau_k)$, the solution of time reparametrizing (TV-flow), Eq. (R-TV-flow), has two main orthogonal modes, ξ_1^k, ξ_2^k , with eigenvalues zero and minus one.*

Proof Substituting Eq. (32) into Eq. (30), we get

$$\begin{aligned} \psi(t(\tau)) &= \sum_{i=k}^L (1 + \lambda_i t(\tau)) \varphi_i, & \forall t \in [T_{k-1}, T_k) \\ &= \sum_{i=k}^L (1 + \lambda_i (a_k e^{-\tau} - c_k)) \varphi_i, & \forall \tau \in [\tau_{k-1}, \tau_k) \\ &= \underbrace{\sum_{i=k}^L \varphi_i - c_k \sum_{i=k}^L \lambda_i \varphi_i}_{\xi_1^k} + e^{-\tau} \underbrace{a_k \sum_{i=k}^L \lambda_i \varphi_i}_{\xi_2^k} = \xi_1^k + e^{-\tau} \xi_2^k, \forall \tau \in [\tau_{k-1}, \tau_k). \end{aligned}$$

By plugging c_k from Eq. (32) into ξ_1^k, ξ_2^k their orthogonality is concluded immediately. \square

3.3 Analysis of the Rescaled-DMD

Here, we show a closed form solution to the time Rescaled-DMD (R-DMD). The common thread in the following discussion is *Attribute 6*, the orthogonality of the TV-spectral components. The method is summarized in Algorithm 3.

Theorem 1 (R-DMD of TV-flow) *Let τ_0 be zero, then for the interval, $[\tau_{k-1}, \tau_k)$, where $k = 1, \dots, L-1$, R-DMD reveals two non-zero orthogonal modes that reconstruct accurately the TV-flow in this interval. For the last interval, $[\tau_{L-1}, \tau_L)$, there is only one nonzero mode.*

Proof According to Prop. 2 and since DMD is an exponential data fitting algorithm, the DMD of the dynamics, Eq. (**R-TV-flow**), is as follows. The modes are $\phi_1^k = \xi_1^k / \|\xi_1^k\|$, $\phi_2^k = \xi_2^k / \|\xi_2^k\|$, and the coefficients are $\alpha_1^k = \|\xi_1^k\|$ and $\alpha_2^k = \|\xi_2^k\|$. Note that one mode is constant with respect to time and the second decays exponentially. Therefore, the eigenvalues are $\mu_1^k = 1$ for the constant mode and $\mu_2^k = e^{-dt}$ where dt is the sampling step size (see Algo. 3). \square

Algorithm 3 R-DMD for TV-flow

- 1: **Inputs:** The initial condition f , and sampling step size dt .
 - 2: **Initialize:** Evolve the solution of (**R-TV-flow**) uniformly with a step size dt .
 - 3: Invoke Algo. 2 with the input f - the result is \mathcal{T} and \mathcal{P} .
 - 4: Map the set of transition time points, \mathcal{T} , to a new set $\hat{\mathcal{T}}$ (Eq. (31)).
 - 5: **for** Every time segment $[\tau_i, \tau_{i+1})$, $\tau_i, \tau_{i+1} \in \hat{\mathcal{T}}$ **do**
 - 6: Invoke the classic DMD with $r = 2$ (when $i = L - 1$, $r = 1$) [31].
 - 7: **end for**
 - 8: **Outputs:** Modes $\{\phi_1^k, \phi_2^k\}_{k=1}^L$, coefficients $\{\alpha_1^k, \alpha_2^k\}_{k=1}^L$, and eigenvalues $\mu_1^k = 1, \mu_2^k = e^{-dt}$.
-

Now we formulate the relation between the TV spectral components φ_k and the R-DMD modes.

Proposition 3 (Revealing TV spectral components from R-DMD)

Given the result of Algo. 3, we can formulate the k th spectral component, φ_k , (Eq. (25)) by the following relation,

$$a_k \lambda_k \varphi_k = \alpha_2^k \phi_2^k - \frac{\langle \alpha_2^k \phi_2^k, \alpha_2^{k+1} \phi_2^{k+1} \rangle}{\|\alpha_2^{k+1} \phi_2^{k+1}\|^2} \alpha_2^{k+1} \phi_2^{k+1}. \quad (33)$$

Proof

$$\begin{aligned} \alpha_2^k \phi_2^k - \frac{\langle \alpha_2^k \phi_2^k, \alpha_2^{k+1} \phi_2^{k+1} \rangle}{\|\alpha_2^{k+1} \phi_2^{k+1}\|^2} \alpha_2^{k+1} \phi_2^{k+1} &= \xi_2^k - \frac{\langle \xi_2^k, \xi_2^{k+1} \rangle}{\|\xi_2^{k+1}\|^2} \xi_2^{k+1} = \\ &= a_k \sum_{i=k}^L \lambda_i \varphi_i - \frac{\langle a_k \sum_{i=k}^L \lambda_i \varphi_i, a_{k+1} \sum_{i=k+1}^L \lambda_i \varphi_i \rangle}{\|a_{k+1} \sum_{i=k+1}^L \lambda_i \varphi_i\|^2} a_{k+1} \sum_{i=k+1}^L \lambda_i \varphi_i \\ &= a_k \lambda_k \varphi_k + \\ &\quad a_k \sum_{i=k+1}^L \lambda_i \varphi_i - a_k \frac{\langle \lambda_k \varphi_k + \sum_{i=k+1}^L \lambda_i \varphi_i, \sum_{i=k+1}^L \lambda_i \varphi_i \rangle}{\|\sum_{i=k+1}^L \lambda_i \varphi_i\|^2} \sum_{i=k+1}^L \lambda_i \varphi_i \\ &= a_k \lambda_k \varphi_k. \quad \square \end{aligned}$$

3.4 Decay profile decomposition with Koopman modes of the TV flow

RDMD can be a solution for homogeneous flows when the dynamics belongs to C^1 . However, it is limited when the dynamics is in C^0 almost everywhere [18]. The attribute of C^0 a.e. is equivalent to the fact that the Koopman modes do not exist during the entire dynamics.

Under the assumption that the dynamical system has a typical monotonic decay profile, a new method was suggested to find the Koopman modes [18]. We summarize this algorithm in Section 2.4. Now, we would like to apply this method on TV-flow. The typical decay profile of zero-homogeneous flows, such as TV-flow, is a linear function (see Eq. (25)), and can be formulated as

$$a_\lambda(t) = (1 + \lambda t)^+ . \quad (34)$$

Denoting the step size as dt , we can formulate the dictionary, D , as

$$D = \begin{bmatrix} 1 & (1 + \lambda_1 dt) & \cdots \\ & \vdots & \\ 1 & (1 + \lambda_N dt) & \cdots \end{bmatrix} . \quad (35)$$

The goal is to find a sparse matrix V such that

$$\Psi \approx VD . \quad (36)$$

4 A Two Dimensional Approximation of TV-flow

We now suggest a way to extend our fast algorithm (FGD) to two dimensions, approximating the anisotropic flow. Anisotropic TV plays an important role in mitigating edge sparsity required by many image processing applications, such as deconvolution, denoising, MRI construction [28], and image segmentation [8, 34]. There are previous approximations of 2D anisotropic TV minimizations, such as [14]. However, there has been little research on fast TV-flow. Until now, a common practice is to solve a nonsmooth convex minimization problem at each time step (using *Alternating Direction Method of Multipliers* (ADMM), primal dual or other methods). This is very inefficient, naturally. Applying our proposed FGD algorithm can accelerate the process tremendously.

Anisotropic TV. The anisotropic TV is defined as follows,

$$J_{ani}(\psi) = \langle \|\nabla\psi\|_1, 1 \rangle = \langle |D_x\psi| + |D_y\psi|, 1 \rangle . \quad (37)$$

We can calculate the subgradient of every column and row with Algo. 1. However, some of the properties of the 1D TV-flow are not valid in 2D. For example, the computation for the next merge event in a row is corrupted by the subgradient of a column. Therefore, we cannot update the subgradient with Algo. 2 and we should repeatedly compute the subgradient with Algo. 1.

Let $P^{(x)}$ be a matrix whose rows are the corresponding negative subgradients of the rows of ψ . Similarly, $P^{(y)}$ contains the negative subgradients of

the columns of ψ . We assume that $P^{(x)} + P^{(y)} = 0$ for every entry iff $P^{(x)} = 0$ and $P^{(y)} = 0$. Namely, it is most likely that the gradient descent flows of TV in x and y axes do not exactly cancel each other. The explicit scheme of the gradient descent flow is given by,

$$\psi_{k+1} = \psi_k + \left(P_k^{(x)} + P_k^{(y)} \right) dt_k, \quad \psi_0 = f, \quad (38)$$

where $P_k^{(x)}$ and $P_k^{(y)}$ denote the subgradients of ψ_k . The constraint on the step size dt_k for which this explicit scheme converges is formulated in the following theorem.

Theorem 2 (Convergence of the explicit scheme) *Let us define the following ratio,*

$$\tilde{\lambda}_k = \frac{\left\| P_k^{(x)} + P_k^{(y)} \right\|^2}{J_{ani}(\psi_k)}, \quad (39)$$

where $J_{ani}(\psi_k)$ is the anisotropic TV of ψ_k . For any time step dt_k admitting,

$$dt_k = \frac{\delta}{\tilde{\lambda}_k}, \quad (40)$$

where $\delta \in (0, 2)$, the explicit scheme, Eq. (38), converges to steady state.

Proof Let us examine the evolution of the ℓ^2 norm of ψ_k under the anisotropic TV-flow. We can formulate the norm of ψ_{k+1} as

$$\begin{aligned} \|\psi_{k+1}\|^2 &= \left\| \psi_k + \left(P_k^{(x)} + P_k^{(y)} \right) dt_k \right\|^2 \\ &= \|\psi_k\|^2 + 2\langle \psi_k, P_k^{(x)} + P_k^{(y)} \rangle dt_k + \left\| \left(P_k^{(x)} + P_k^{(y)} \right) \right\|^2 \cdot dt_k^2 \\ &= \|\psi_k\|^2 + 2\langle \psi_k, P_k^{(x)} + P_k^{(y)} \rangle \delta \frac{J_{ani}(\psi_k)}{\left\| P_k^{(x)} + P_k^{(y)} \right\|^2} \\ &\quad + \left\| P_k^{(x)} + P_k^{(y)} \right\|^2 \cdot \delta^2 \frac{J(\psi_k)^2}{\left\| P_k^{(x)} + P_k^{(y)} \right\|^4} \\ &= \|\psi_k\|^2 - 2\delta \frac{J_{ani}(\psi_k)^2}{\left\| P_k^{(x)} + P_k^{(y)} \right\|^2} + \delta^2 \frac{J_{ani}(\psi_k)^2}{\left\| P_k^{(x)} + P_k^{(y)} \right\|^2} \\ &= \|\psi_k\|^2 + (\delta^2 - 2\delta) \frac{J_{ani}(\psi_k)^2}{\left\| P_k^{(x)} + P_k^{(y)} \right\|^2} \end{aligned} \quad (41)$$

Since $\delta \in (0, 2)$, $\|\psi_{k+1}\|^2 - \|\psi_k\|^2 \leq 0$. Then, the series $\{\|\psi_k\|\}^2$ is monotonically decreasing and bounded from below by zero, therefore converges. Then, the difference between two successive elements converges to zero. Since the term $\delta^2 - 2\delta$ is constant then the ratio $\frac{J_{ani}(\psi_k)^2}{\left\| P_k^{(x)} + P_k^{(y)} \right\|^2}$ converges to zero. In addition, the denominator is bounded from above, therefore, $J(\psi_k) \rightarrow 0$ as $k \rightarrow \infty$.

5 Results

In this section, we illustrate the theory and algorithms discussed above. We use standard first-order discretization of the derivatives and Neumann boundary conditions.

5.1 1D results

We begin with a toy example, depicted in Fig. 2a. We show that the solution of (**TV-flow**) decays linearly (Fig. 2b) and that of Eq. (**R-TV-flow**) piecewise exponentially, (Fig. 2c).

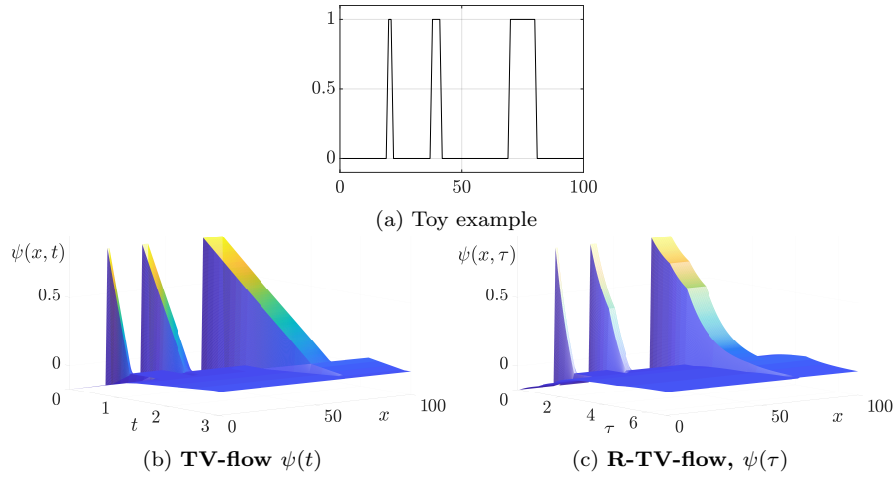


Fig. 2: **Time reparametrization** - (a) **The initial condition** is a signal with three pulses with different widths. (b) **TV-flow** $\psi(t)$ decays piecewise linearly. (c) **R-TV-flow**, $\psi(t)$ is mapped to a piecewise smooth function.

The non-smooth points represent transitions in the subgradient.

In Fig. 3 we show the TV-modes defined in Prop. 2 with the initial condition Fig. 2a. It contains six disjoint intervals with the corresponding modes $\{\xi_1^k, \xi_2^k\}_{k=1}^6$.

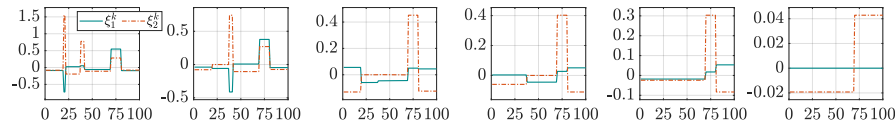


Fig. 3: Modes: ξ_1^k (teal) - constant, ξ_2^k (orange) - exponentially decaying.

In Fig. 4-top the TV-spectral decomposition, dashed red line (computed in the standard way, see [23]) is compared with two algorithms: Algorithm 3 based on Prop. 3, black dotted line, and Algorithm 2, blue line. The errors between the TV-spectral decomposition and Algorithms 3 and 2 are depicted in Fig. 4-bottom. We can observe an excellent match in both cases.

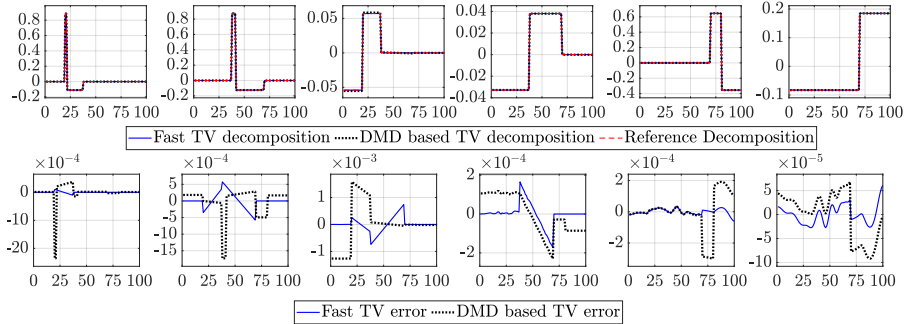


Fig. 4: **TV spectral decomposition comparison for toy example** - The standard method of spectral decomposition (Dashed red line) vs. fast TV decomposition and R-DMD decomposition in blue and dotted black lines respectively. Bottom row - respective errors

In Fig. 5, we show results of the fast TV-spectral decomposition, Algorithm 2, applied on a natural signal. We arbitrarily chose the red line from the zebra in Fig. 5a, depicted in Fig. 5b. Bands of standard TV-spectral decomposition and the fast TV-spectral decomposition are shown in Fig. 5c. One can observe that our proposed fast method recovers the spectral bands faithfully, with negligible error, Fig. 5d.

Rough performance comparison. We report the elapsed time in seconds, running in Matlab 2018b on an 8th Gen. Core i7 laptop with 16GB RAM. Initial condition Fig. 2a: Standard method (iterative application of [11]) - 488.4s; ours - 0.013s. Initial condition Fig. 5b (zebra): Standard method - 7.1×10^3 s; ours - 0.15s.

5.2 2D results

Here we compare between isotropic and anisotropic TV-spectral decomposition and between the TV-spectral decomposition and the decay profile decomposition with Koopman modes (36). The Anisotropic TV-Flow is computed by the accelerated flow based on Theorem 2. The algorithm to approximate the Koopman mode is dictated by the typical decay profile and formulated in 3.4.

In Fig. 6a, we show the isotropic TV spectral decomposition of the Zebra from Fig. 5a. In Figs. 6b–6e, we show the decomposition according to the per-

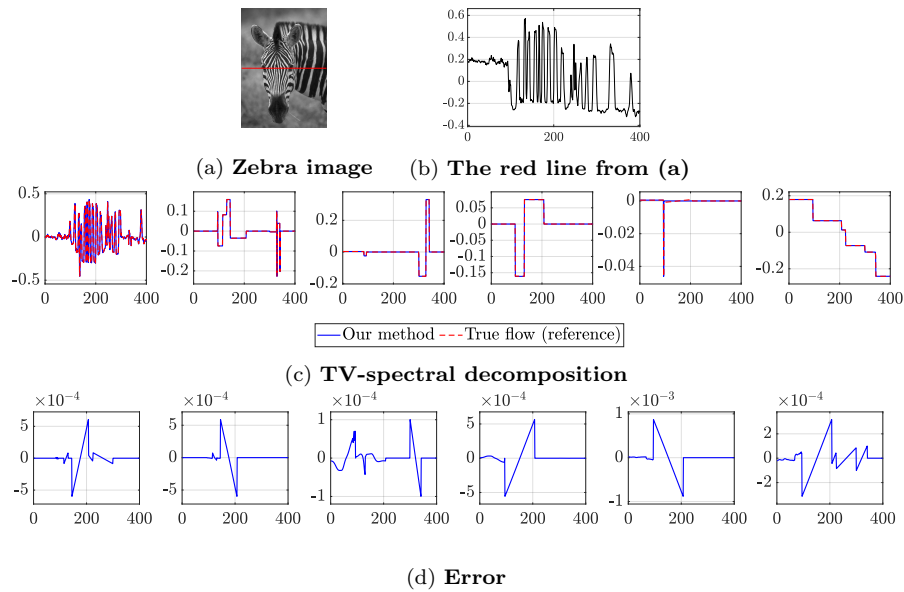


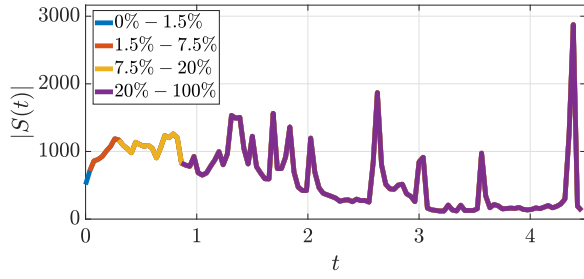
Fig. 5: **TV spectral decomposition comparison for an arbitrary initial condition** - (b) The corresponding values of the pixels on the red line in (a). (c) Standard method of spectral decomposition (Dashed red line) vs. fast TV decomposition (Blue line). (d) The respective error.

centage depicted in Fig. 6a. In Fig. 7, we present the decomposition results to the same band separation, but this time based on Eq. (36). From a qualitative perspective, a very similar decomposition is obtained.

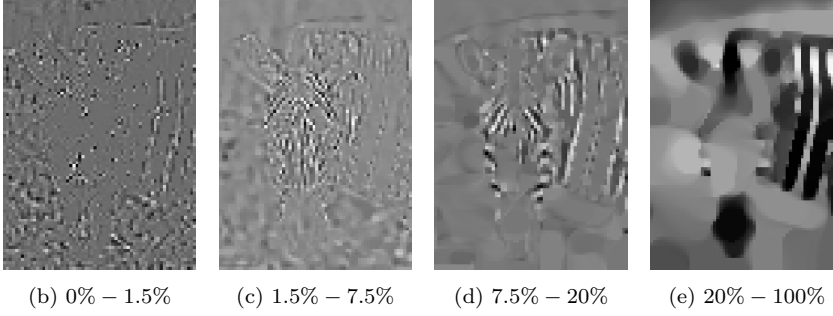
In Fig. 8a, the anisotropic TV-spectrum is presented and the decomposition according to the percentage in 8a is depicted in Figs. 8b–8e. We show the corresponding decay profile decomposition in Fig. 9

6 Conclusion

In this paper we thoroughly examined the DMD[31] algorithm and Koopman Theory as tools for spectral analysis and decomposition of the TV-flow. We proposed the *Rescaled Dynamic Mode Decomposition* (RDMD) adaptation as a means to overcome difficulties in DMD application due to the linear-decay nature of the TV flow. We have found exact relations between TV spectral decomposition, the *Koopman Mode Decomposition* (KMD) algorithm and DMD. Due to the discontinuity of the dynamic, a decomposition based on the decay profile [18] is called for. We applied this decomposition to separate the flow into Koopman modes, to compare them against the original TV spectral decomposition.



(a) The isotropic TV-spectrum vs. time



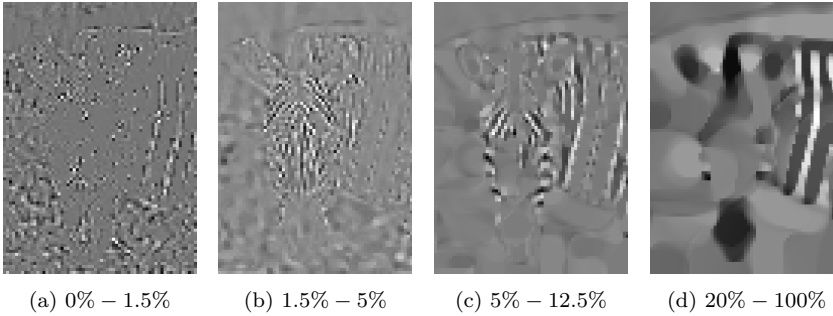
(b) 0% - 1.5%

(c) 1.5% - 7.5%

(d) 7.5% - 20%

(e) 20% - 100%

Fig. 6: Zebra image isotropic TV-decomposition



(a) 0% - 1.5%

(b) 1.5% - 5%

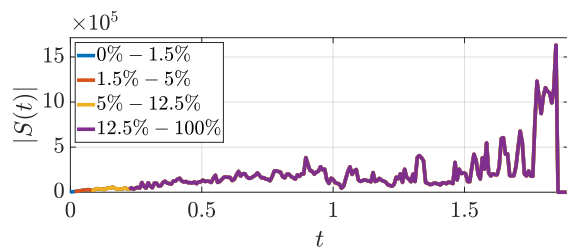
(c) 5% - 12.5%

(d) 20% - 100%

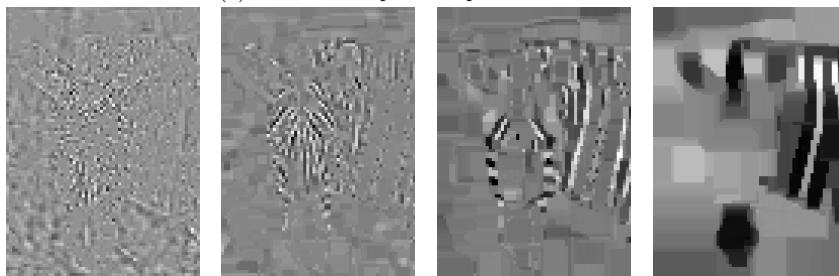
Fig. 7: Zebra image - decay profile decomposition with Koopman modes of isotropic TV flow

Since evolving TV-flow is a slow process using optimization techniques, we have proposed a very fast method, based on simple updates of the sub-gradient. Finally, our accelerated algorithm was extended for solving the two-dimensional anisotropic TV-Flow.

Acknowledgements. This work was supported by the European Union's Horizon 2020 research and innovation programme under the Marie Skłodowska-Curie grant agreement No. 777826 (NoMADS). GG acknowledges support by the Israel Science Foundation (Grant No. 534/19) and by the Ollendorff Minerva Center.



(a) The anisotropic TV-spectrum vs. time



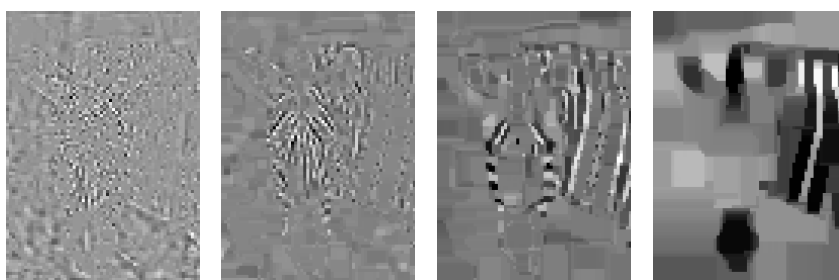
(b) 0% - 1.5%

(c) 1.5% - 5%

(d) 5% - 12.5%

(e) 20% - 100%

Fig. 8: Zebra image anisotropic TV-decomposition, computed by the accelerated flow, Theorem 2 and Algo. 1.



(a) 0% - 1.5%

(b) 1.5% - 5%

(c) 5% - 12.5%

(d) 20% - 100%

Fig. 9: Zebra image - decay profile decomposition with Koopman modes of anisotropic TV flow, computed by the accelerated flow, Theorem 2 and Algo. 1.

References

1. Andreu, F., Ballester, C., Caselles, V., Mazón, J.M.: Minimizing total variation flow. *Differential and Integral Equations* **14**(3), 321–360 (2001)
2. Askham, T., Kutz, J.N.: Variable projection methods for an optimized dynamic mode decomposition. *SIAM Journal on Appl. Dyn. Sys.* **17**(1), 380–416 (2018)
3. Bellettini, G., Caselles, V., Novaga, M.: The total variation flow in \mathbb{R}^n . *Journal of Differential Equations* **184**(2), 475–525 (2002)

4. Bonforte, M., Figalli, A.: Total variation flow and sign fast diffusion in one dimension. *Journal of Differential Equations* **252**(8), 4455–4480 (2012)
5. Brokman, J., Gilboa, G.: Nonlinear spectral processing of shapes via zero-homogeneous flows. In: A. Elmoataz, J. Fadili, Y. Quéau, J. Rabin, L. Simon (eds.) *Scale Space and Variational Methods in Computer Vision*, pp. 40–51. Springer International Publishing, Cham (2021)
6. Brox, T., Weickert, J.: A TV flow based local scale estimate and its application to texture discrimination. *J. of Vis. Comm. and Image Rep.* **17**(5), 1053–1073 (2006)
7. Brox, T., Welk, M., Steidl, G., Weickert, J.: Equivalence results for tv diffusion and tv regularisation. In: *International Conference on Scale-Space Theories in Computer Vision*, pp. 86–100. Springer (2003)
8. Bui, K., Park, F., Lou, Y., Xin, J.: A weighted difference of anisotropic and isotropic total variation for relaxed mumford–shah color and multiphase image segmentation. *SIAM Journal on Imaging Sciences* **14**(3), 1078–1113 (2021)
9. Bungert, L., Burger, M., Chambolle, A., Novaga, M.: Nonlinear spectral decompositions by gradient flows of one-homogeneous functionals. *Analysis & PDE* **14**(3), 823–860 (2021)
10. Burger, M., Gilboa, G., Moeller, M., Eckardt, L., Cremers, D.: Spectral decompositions using one-homogeneous functionals. *SIAM Im. Sci.* **9**(3), 1374–1408 (2016)
11. Chambolle, A.: An algorithm for total variation minimization and applications. *Journal of Mathematical imaging and vision* **20**(1-2), 89–97 (2004)
12. Chambolle, A., Caselles, V., Cremers, D., Novaga, M., Pock, T.: An introduction to total variation for image analysis. *Theoretical foundations and numerical methods for sparse recovery* **9**(263-340), 227 (2010)
13. Cherkaoui, H., Sulam, J., Moreau, T.: Learning to solve tv regularised problems with unrolled algorithms. *Adv. Neural Inf. Proc. Sys.* **33** (2020)
14. Choksi, R., van Gennip, Y., Oberman, A.: Anisotropic total variation regularized l^1 approximation and denoising/deblurring of 2d bar codes. *Inverse Problems & Imaging* **5**(3), 591 (2011)
15. Cohen, I., Azencot, O., Lifshits, P., Gilboa, G.: Modes of homogeneous gradient flows. *arXiv preprint arXiv:2007.01534* (2020)
16. Cohen, I., Berkov, T., Gilboa, G.: Total-variation mode decomposition. In: A. Elmoataz, J. Fadili, Y. Quéau, J. Rabin, L. Simon (eds.) *Scale Space and Variational Methods in Computer Vision*, pp. 52–64. Springer International Publishing, Cham (2021)
17. Cohen, I., Gilboa, G.: Introducing the p-laplacian spectra. *Signal Processing* **167**, 107281 (2020)
18. Cohen, I., Gilboa, G.: Examining the limitations of dynamic mode decomposition through koopman theory analysis. *arXiv preprint arXiv:2107.07456* (2021)
19. Darbon, J., Sigelle, M.: Image restoration with discrete constrained total variation part i: Fast and exact optimization. *J. Math. Im. and Vision* **26**(3), 261–276 (2006)
20. Elmore, C.T., Dowling, A.W.: Learning spatiotemporal dynamics in wholesale energy markets with dynamic mode decomposition. *Energy* p. 121013 (2021)
21. Fumero, M., Möller, M., Rodolà, E.: Nonlinear spectral geometry processing via the tv transform. *ACM Transactions on Graphics (TOG)* **39**(6), 1–16 (2020)
22. Gilboa, G.: A spectral approach to total variation. In: *Inter. Conf. on Scale Space and Variational Methods in Computer Vision*, pp. 36–47. Springer (2013)
23. Gilboa, G.: A total variation spectral framework for scale and texture analysis. *SIAM journal on Imaging Sciences* **7**(4), 1937–1961 (2014)
24. Gilboa, G., Moeller, M., Burger, M.: Nonlinear spectral analysis via one-homogeneous functionals: Overview and future prospects. *Journal of Mathematical Imaging and Vision* **56**(2), 300–319 (2016)
25. Goldfarb, D., Yin, W.: Parametric maximum flow algorithms for fast total variation minimization. *SIAM J. Sci. Comp.* **31**(5), 3712–3743 (2009)
26. Koopman, B.O.: Hamiltonian systems and transformation in hilbert space. *Proceedings of the national academy of sciences of the united states of america* **17**(5), 315 (1931)
27. Kuijper, A.: p-laplacian driven image processing. In: *2007 IEEE International Conference on Image Processing*, vol. 5, pp. V–257. IEEE (2007)

28. Lou, Y., Zeng, T., Osher, S., Xin, J.: A weighted difference of anisotropic and isotropic total variation model for image processing. *SIAM Journal on Imaging Sciences* **8**(3), 1798–1823 (2015)
29. Mezić, I.: Spectral properties of dynamical systems, model reduction and decompositions. *Nonlinear Dynamics* **41**(1-3), 309–325 (2005)
30. Rosenfeld, J.A., Kamalapurkar, R.: Singular dynamic mode decompositions. *arXiv preprint arXiv:2106.02639* (2021)
31. Schmid, P.J.: Dynamic mode decomposition of numerical and experimental data. *Journal of fluid mechanics* **656**, 5–28 (2010)
32. Steidl, G., Didas, S., Neumann, J.: Relations between higher order TV regularization and support vector regression. In: *Inter. Conf. on Scale-Space Theories in Computer Vision*, pp. 515–527. Springer (2005)
33. Steidl, G., Weickert, J., Brox, T., Mrázek, P., Welk, M.: On the equivalence of soft wavelet shrinkage, total variation diffusion, total variation regularization, and sides. *SIAM J. on Num. Ana.* **42**(2), 686–713 (2004)
34. Wu, T., Gu, X., Wang, Y., Zeng, T.: Adaptive total variation based image segmentation with semi-proximal alternating minimization. *Signal Processing* **183**, 108017 (2021)
35. Zhang, H., Dawson, S.T., Rowley, C.W., Deem, E.A., Cattafesta, L.N.: Evaluating the accuracy of the dynamic mode decomposition. *Journal of Computational Dynamics* **7**(1), 35–56 (2020)